

Calibrating Bayesian Learning via Regularization, Confidence Minimization, and Selective Inference

Jiayi Huang, Sangwoo Park, *Member, IEEE*, and Osvaldo Simeone, *Fellow, IEEE*

Abstract

The application of artificial intelligence (AI) models in fields such as engineering is limited by the known difficulty of quantifying the reliability of an AI's decision. A well-calibrated AI model must correctly report its accuracy on in-distribution (ID) inputs, while also enabling the detection of out-of-distribution (OOD) inputs. A conventional approach to improve calibration is the application of Bayesian ensembling. However, owing to computational limitations and model misspecification, practical ensembling strategies do not necessarily enhance calibration. This paper proposes an extension of variational inference (VI)-based Bayesian learning that integrates calibration regularization for improved ID performance, confidence minimization for OOD detection, and selective calibration to ensure a synergistic use of calibration regularization and confidence minimization. The scheme is constructed successively by first introducing calibration-regularized Bayesian learning (CBNN), then incorporating out-of-distribution confidence minimization (OCM) to yield CBNN-OCM, and finally integrating also selective calibration to produce selective CBNN-OCM (SCBNN-OCM). Selective calibration rejects inputs for which the calibration performance is expected to be insufficient. Numerical results illustrate the trade-offs between ID accuracy, ID calibration, and OOD calibration attained by both frequentist and Bayesian learning methods. Among the main conclusions, SCBNN-OCM is seen to achieve best ID and OOD performance as compared to existing state-of-the-art approaches at the cost of rejecting a sufficiently large number of inputs.

The authors are with the King's Communications, Learning & Information Processing (KCLIP) lab within the Centre for Intelligent Information Processing Systems (CIIPS), Department of Engineering, King's College London, London WC2R 2LS, U.K. (e-mail: {jiayi.3.huang, sangwoo.park, osvaldo.simeone}@kcl.ac.uk).

The work of J. Huang was supported by the King's College London and China Scholarship Council for their Joint Full-Scholarship (K-CSC) (grant agreement No. 202206150005). The work of O. Simeone was supported by European Union's Horizon Europe project CENTRIC (101096379), by the Open Fellowships of the EPSRC (EP/W024101/1), by the EPSRC project (EP/X011852/1), and by Project REASON, a UK Government funded project under the Future Open Networks Research Challenge (FONRC) sponsored by the Department of Science Innovation and Technology (DSIT).

Index Terms

Bayesian learning, calibration, OOD detection, selective calibration

I. INTRODUCTION

A. Context and Motivation

Modern artificial intelligence (AI) models, including deep neural networks and large language models, have achieved great success in many domains, even surpassing human experts in specific tasks [1]. However, it is common to hear concerns voiced by experts on the application of AI for safety-critical fields such as engineering [2] or health care [3]. These concerns hinge on the known difficulty in quantifying the reliability of an AI’s decision, as in the well-reported phenomenon of the “hallucinations” of large language models [4]–[7]. Indeed, in safety-critical applications, *calibration* – i.e., the property of a model to know when it does not know – is arguably just as important as accuracy [8]–[11].

A well-calibrated AI model must correctly report its accuracy on *in-distribution* (ID) inputs, i.e., on inputs following the same statistics as training data, while also enabling the detection of *out-of-distribution* (OOD) inputs, i.e., of inputs that are not covered by the training data distribution.

A conventional approach to improve ID calibration is the application of Bayesian *ensembling*. A *Bayesian neural network* (BNN) captures epistemic uncertainty via a distribution over the weights of the model, making it possible to evaluate reliability via the level of consensus between models drawn from the model distribution [2], [12]–[14]. However, owing to computational limitations and model misspecification, practical ensembling strategies do not necessarily enhance ID calibration [15]–[19]. Furthermore, improvements in ID calibration may not necessarily improve OOD detection [2], [20], [21].

This paper proposes an extension of *variational inference* (VI)-based Bayesian learning that integrates calibration regularization for improved ID performance [22], confidence minimization for enhanced OOD detection [23], and selective calibration to ensure a synergistic use of calibration regularization and confidence minimization [24]. Prior art only considered the separate applications of these techniques to conventional *frequentist neural networks* (FNNs), and, to the best of our knowledge, no study has been done on integrating the three approaches and on adapting them for use in the training of BNNs.

B. State of the Art

As shown in Fig. 1(a), conventional FNNs do not capture epistemic uncertainty, i.e., the uncertainty that arises due to limited access to training data. As a result, they often fail to provide a reliable quantification of uncertainty for both ID data – i.e., in between data points – and OOD data – i.e., away from the domain spanned by training data [25], [26]. OOD calibration is measured in terms of the capacity of the model to detect inputs that are too different from available training data, which requires the capacity to measure epistemic uncertainty [21], [27].

In order to enhance the ID calibration of FNNs, *calibration regularization* modifies the training loss by adding measures of ID calibration, such as the *maximum mean calibration error* (MMCE) [22], the *ESD* [28], the *focal loss* [29], and the *soft AvUC* [30]. As shown in Fig. 1(b), FNNs with calibration regularization can improve ID calibration, but it does not resolve the issue that FNNs cannot model epistemic uncertainty, as they treat model weights as deterministic quantities, rather than as random variables in BNNs.

As mentioned, improving ID calibration does not necessarily enhance OOD detection, and tailored methods are required for this purpose [2], [12], [13], [23], [27], [31]. As illustrated in Fig. 1(c), *out-of-distribution confidence minimization* (OCM) augments the data set with OOD inputs, which are used to specify a regularizer that favors high uncertainty outside the training set [23]. However, in so doing, OCM can hurt ID calibration, making the model excessively conservative.

Overall, there is generally a trade-off between OOD and ID calibration, and schemes designed to optimize either criterion may hurt the other [23]. A possible solution to this problem is to properly select inputs on which to make a decision. *Selective inference* techniques typically focus on enhancing the accuracy of the model by selecting inputs with the largest model confidence among the selected inputs [24], [32], [32]–[35]. As a result, these techniques may end up exacerbating issues with ID calibration by favoring over-confidence. In contrast, as shown in Fig. 1(d), *selective calibration* learns how to select inputs that are expected to have a low gap between accuracy and confidence, thus boosting ID calibration [24].

All the papers presented so far have focused on improving ID and OOD calibration for FNNs, and are thus limited in the capacity to provide reliable decisions that fully account for epistemic uncertainty.

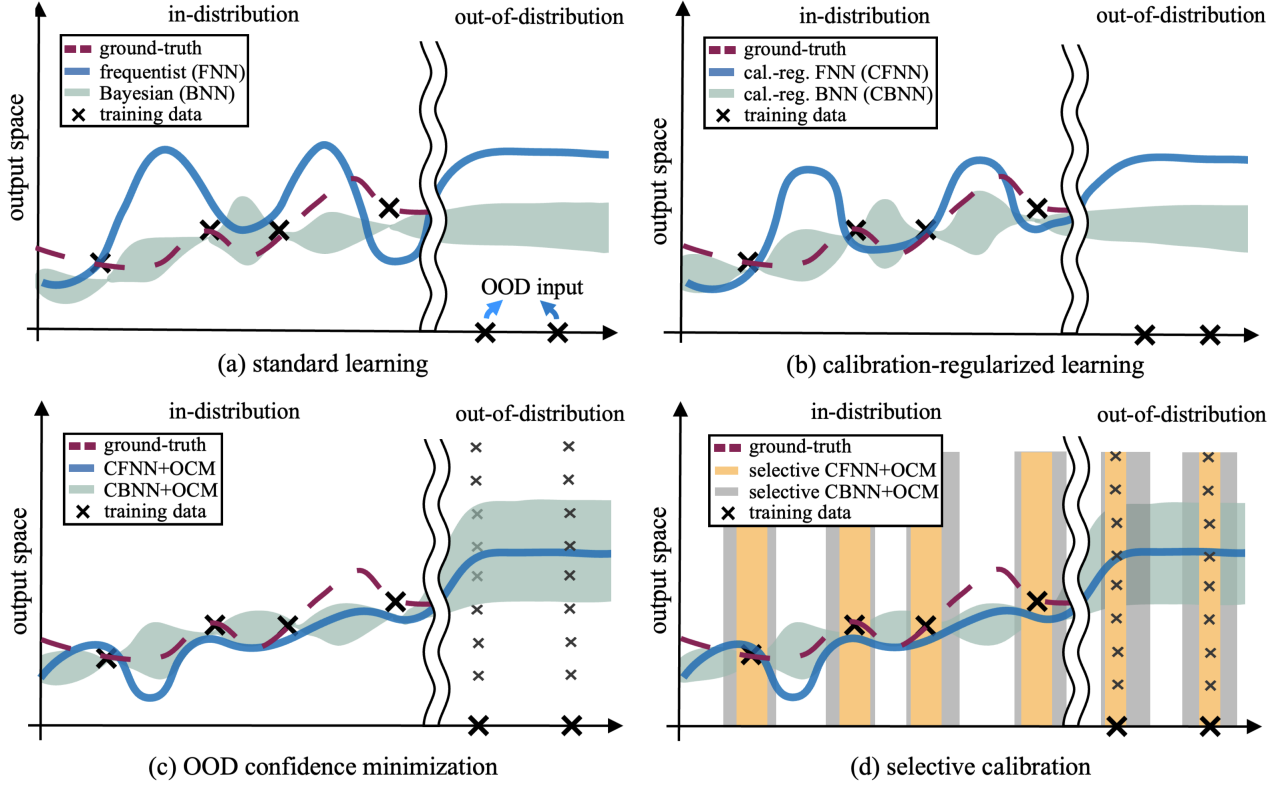


Fig. 1. (a) Standard frequentist neural networks (FNNs) generally fail to provide well-calibrated decisions, and improved in-distribution (ID) calibration can be achieved via Bayesian neural networks (BNNs) [36]. (b) *Calibration regularization* improves ID calibration via a regularizer that penalizes calibration errors [22]. (c) *Out-of-distribution confidence minimization* (OCM) injects OOD examples during training to improve OOD detection [23]. (d) *Selective calibration* further improves both ID and OOD calibration by only producing decisions for inputs at which uncertainty quantification is deemed to be sufficiently reliable. Prior works [22]–[24] introduced calibration regularization, OCM, and selective calibration as separate methods for FNNs, while this work presents an integrated approach encompassing all three solutions for BNNs.

C. Main Contributions

This paper proposes an extension of VI-based BNN learning that integrates calibration regularization for improved ID performance, OCM for OOD detection, and selective calibration to ensure a synergistic use of calibration regularization and OCM. As illustrated in Fig. 1, the scheme is constructed successively by first introducing calibration-regularized Bayesian learning (CBNN), then incorporating OCM to yield CBNN-OCM, and finally integrating also selective calibration to produce selective CBNN-OCM (SCBNN-OCM).

Overall, the main contributions are as follows.

- We propose CBNN, a novel variant of VI-based BNNs that improve the ID calibration

performance in the presence of computational complexity constraints and model misspecification by adding a calibration-aware regularizer (see Fig. 1(b)).

- In order to improve OOD detection, CBNN is extended via OCM, yielding CBNN-OCM, by incorporating an additional regularizer that penalizes confidence on OOD data (see Fig. 1(c)).
- Since CBNN-OCM can enhance OOD detection performance at the cost of ID performance, we finally propose to further generalize CBNN-OCM via selective calibration (see Fig. 1(d)). The proposed scheme, SCBNN-OCM, selects inputs that are likely to be well calibrated, avoiding inputs whose ID calibration may have been damaged by OCM.
- Extensive experimental results on real-world image classification task, including CIFAR-100 data set [37] and TinyImageNet data set [38], illustrate the trade-offs between ID accuracy, ID calibration, and OOD calibration attained by both FNN and BNN. Among the main conclusions, SCBNN-OCM is seen to achieve best ID and OOD performance as compared to existing state-of-the-art approaches at the cost of rejecting a sufficiently large number of inputs.

A table summarizing the comparison of our paper to existing studies can be found in Table I. In this regard, it is noted that preliminary results on CBNN were presented in the conference version [36] of this paper. Also related is reference [13], which presented a version of CBNN that includes a calibration-aware regularization term, AvUC, whose limitation as a calibration-aware regularizer were demonstrated in [30].

The remainder of the paper is organized as follows. Sec. II summarizes necessary background on ID calibration, calibration-aware training, and Bayesian learning, and it presents CBNN. OOD detection is discussed in Sec. III, which introduces CBNN-OCM. Sec. IV describes the selective calibration, and proposes SCBNN-OCM. Sec. V illustrates experimental setting and results. Finally, Sec. VI concludes the paper.

II. CALIBRATION-REGULARIZED BAYESIAN LEARNING

In this section, we aim at improving the calibration performance of BNNs by introducing a data-dependent regularizer that penalizes calibration errors (see Fig. 1(b)). The approach extends the *calibration-regularized FNNs* (CFNNs) of [22] to CBNNs. We start by defining calibration for classification tasks, followed by a summary of frequentist learning and Bayesian learning. Finally, we propose CBNN.

TABLE I
COMPARISON OF MOST RELATED WORKS

reference	learning*	calibration regularization	OOD confidence minimization	selective inference
[22], [28]–[30], [39]	F	✓		
[13], [36]	B	✓		
[23]	F		✓	
[24]	F			✓
ours	F, B	✓	✓	✓

*: “F” and “B” stand for frequentist learning and Bayesian learning, respectively.

A. In-Distribution Calibration

Given a training data set $\mathcal{D}^{\text{tr}} = \{(x_i, y_i)\}_{i=1}^{|\mathcal{D}^{\text{tr}}|}$, with i -th input $x_i \in \mathcal{X}$ and corresponding output $y_i \in \mathcal{Y}$ generated in an independent identically distributed (i.i.d) manner by following an unknown, underlying joint distribution $p(x, y)$, supervised learning for classification optimizes a *probabilistic predictor* $p(y|x, \mathcal{D}^{\text{tr}})$ of output y given input x . A probabilistic predictor outputs a *confidence level* $p(y|x, \mathcal{D}^{\text{tr}})$ for all possible outputs $y \in \mathcal{Y}$ given any input $x \in \mathcal{X}$ and data set \mathcal{D}^{tr} . Given an input x , a *hard* decision \hat{y} can be obtained by choosing the output that has the maximum confidence level, i.e.,

$$\hat{y}(x) = \arg \max_{y' \in \mathcal{Y}} p(y'|x, \mathcal{D}^{\text{tr}}). \quad (1)$$

Furthermore, the probabilistic predictor $p(y(x)|x, \mathcal{D}^{\text{tr}})$ provides a measure of the confidence of the prediction for a given input x as

$$r(x) = p(\hat{y}(x)|x, \mathcal{D}^{\text{tr}}) = \max_{y' \in \mathcal{Y}} p(y'|x, \mathcal{D}^{\text{tr}}). \quad (2)$$

A probabilistic predictor is said to be *perfectly ID calibrated* whenever its average prediction accuracy for any confidence level $r \in [0, 1]$ equals r . This condition is formalized by the equality

$$\Pr [y = \hat{y}|p(\hat{y}|x, \mathcal{D}^{\text{tr}}) = r] = r, \text{ for all } r \in [0, 1], \quad (3)$$

where the probability is taken with respect to the pairs of test data (x, y) . For ID calibration, one specifically assume the test pair (x, y) to follow the same distribution $p(x, y)$ of the training data. Under the perfect ID calibration condition (3), among all input-output pairs (x, y) that have the same confidence level r , the average fraction of correct decisions, with $\hat{y}(x) = y$, equals r .

Importantly, perfect calibration does not imply high accuracy [26], [40]. For instance, if the marginal distribution of the labels $y \in \mathcal{Y}$ is uniform, a model that disregards the input x , assigning a uniform confidence $p(y|x, \mathcal{D}^{\text{tr}}) = 1/|\mathcal{Y}|$, achieves perfect calibration, while offering a generally low accuracy.

The extent to which condition (3) is satisfied is typically evaluated via the *reliability diagram* [41] and the *expected calibration error* (ECE) [25], [42]. Both approaches estimate the probability in (3) using a test data set $\mathcal{D}^{\text{te}} = \{(x_i^{\text{te}}, y_i^{\text{te}})\}_{i=1}^{|\mathcal{D}^{\text{te}}|}$, with each pair $(x_i^{\text{te}}, y_i^{\text{te}}) \sim p(x, y)$ being drawn independently of the training data set \mathcal{D}^{tr} .

As illustrated in Fig. 2, a *reliability diagram* plots the average confidence produced by the model for all inputs with the same confidence level r in (3). By (3), perfect calibration is obtained when the curve is aligned with the diagonal line, i.e., the dashed line in Fig. 2. In contrast, a curve below the diagonal line, e.g., the red line in Fig. 2, indicates over-confidence, while a curve above the diagonal line, such as the green line in Fig. 2, implies an under-confident prediction.

To elaborate further on calibration measure, denote the *confidence score* associated with the i -th test input x_i^{te} as

$$r_i^{\text{te}} = p(\hat{y}_i^{\text{te}}(x_i^{\text{te}})|x_i^{\text{te}}, \mathcal{D}^{\text{tr}}), \quad (4)$$

given the hard decision (1), and the corresponding *accuracy score* as

$$c_i^{\text{te}} = \mathbb{1}(\hat{y}_i^{\text{te}}(x_i^{\text{te}}) = y_i^{\text{te}}), \quad (5)$$

with the indicator function $\mathbb{1}(\cdot)$ defined as $\mathbb{1}(\text{true}) = 1$ and $\mathbb{1}(\text{false}) = 0$. To enable an estimate of the reliability diagram, we partition the test data points into *bins* with approximately the same confidence level (4). Specifically, the m -th bin \mathcal{B}_m contains indices i of the test inputs that have confidence scores lying in the interval $(\frac{m-1}{M}, \frac{m}{M}]$, i.e., $\mathcal{B}_m = \{i \in \{1, \dots, M\} : r_i^{\text{te}} \in (\frac{m-1}{M}, \frac{m}{M}]\}$.

Each m -th bin is associated with a *per-bin confidence* $\text{conf}(\mathcal{B}_m) = 1/|\mathcal{B}_m| \sum_{i \in \mathcal{B}_m} r_i^{\text{te}}$, and with a *per-bin accuracy* $\text{acc}(\mathcal{B}_m) = 1/|\mathcal{B}_m| \sum_{i \in \mathcal{B}_m} c_i^{\text{te}}$. An estimate of the reliability diagram is now obtained by plotting $\text{acc}(\mathcal{B}_m)$ as a function of $\text{conf}(\mathcal{B}_m)$ across all bins $m = 1, \dots, M$.

A scalar calibration metric can be extracted from a reliability diagram by evaluating the average discrepancy between the per-bin confidence $\text{conf}(\mathcal{B}_m)$ and the per-bin accuracy $\text{acc}(\mathcal{B}_m)$. Via weighting the contribution of each bin by the corresponding fraction of samples, the ECE is defined as [42]

$$\text{ECE} = \sum_{m=1}^M \frac{|\mathcal{B}_m|}{\sum_{m'=1}^M |\mathcal{B}_{m'}|} |\text{acc}(\mathcal{B}_m) - \text{conf}(\mathcal{B}_m)|. \quad (6)$$

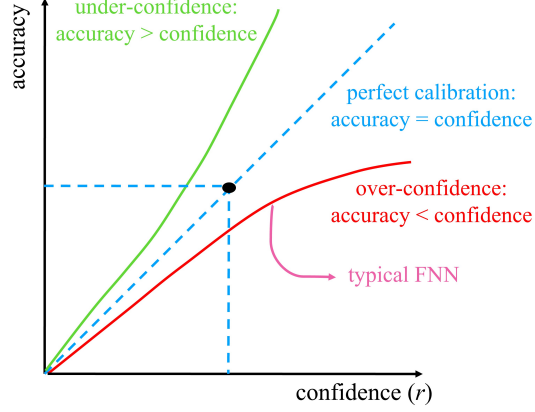


Fig. 2. Reliability diagrams visualize the calibration performance (3) of the model by evaluating the average accuracy over test examples to which the prediction has the same confidence value r . Typically, FNNs return over-confident decisions, for which the accuracy is lower than the confidence obtained by the model.

B. Calibration-Regularized Frequentist Learning

Given a parameterized vector of probabilistic predictor $p(y|x, \theta)$, standard FNN training aims at finding a parameter vector θ^{FNN} that minimizes the training loss $\mathcal{L}(\theta|\mathcal{D}^{\text{tr}})$. The loss function is typically defined as the negative log-likelihood, or cross-entropy, yielding the solution

$$\theta^{\text{FNN}} = \arg \min_{\theta} \left\{ \mathcal{L}(\theta|\mathcal{D}^{\text{tr}}) = - \sum_{(x,y) \in \mathcal{D}^{\text{tr}}} \log p(y|x, \theta) \right\}. \quad (7)$$

Frequentist learning often yields over-confident outputs that fall far short of satisfying the calibration condition (3) [12], [25], [43]. To address this problem, reference [22] proposed to modify the training loss by adding a data-dependent *calibration-based* regularizer, namely MMCE, which is defined as

$$\mathcal{E}(\theta|\mathcal{D}^{\text{tr}}) = \left(\sum_{i=1}^{|\mathcal{D}^{\text{tr}}|} \sum_{j=1}^{|\mathcal{D}^{\text{tr}}|} \frac{(c_i - r_i)(c_j - r_j)\kappa(r_i, r_j)}{|\mathcal{D}^{\text{tr}}|^2} \right)^{\frac{1}{2}}, \quad (8)$$

where $\kappa(\cdot, \cdot)$ is a kernel function. The MMCE (8) provides a differentiable measure of the extent to which the calibration condition (3) is satisfied, and the confidence score r_i and correctness score c_i are defined as in (4) and (5), respectively, with the only difference that they are evaluated based on i -th training example (x_i, y_i) . Other possible choices for the regularizer $\mathcal{E}(\theta|\mathcal{D}^{\text{tr}})$ include the *weighted MMCE* [22], the *differentiable ECE* [39], the *ESD* [28], the *focal loss* [29], and the *soft AvUC* [30].

Equipped with a data-dependent calibration-aware regularizer $\mathcal{E}(\theta|\mathcal{D}^{\text{tr}})$, CFNN aims at finding a deterministic parameter vector θ^{CFNN} that minimizes the regularized cross-entropy loss as per the optimization [22]

$$\theta^{\text{CFNN}} = \arg \min_{\theta} \{ \mathcal{L}(\theta|\mathcal{D}^{\text{tr}}) + \lambda \cdot \mathcal{E}(\theta|\mathcal{D}^{\text{tr}}) \} \quad (9)$$

given a hyperparameter $\lambda > 0$. Accordingly, the trained probabilistic predictor is obtained as

$$p(y|x, \mathcal{D}^{\text{tr}}) = p(y|x, \theta^{\text{CFNN}}). \quad (10)$$

Note that in (9) the regularizer $\mathcal{E}(\theta|\mathcal{D}^{\text{tr}})$ depends on the same training data \mathcal{D}^{tr} used in the cross-entropy loss $\mathcal{L}(\theta|\mathcal{D}^{\text{tr}})$. An alternative, investigated in [28], is to split the training data into two disjoint parts $\mathcal{D}_1^{\text{tr}}$ and $\mathcal{D}_2^{\text{tr}}$ with $\mathcal{D}_1^{\text{tr}} \cup \mathcal{D}_2^{\text{tr}} = \mathcal{D}^{\text{tr}}$ and evaluate the regularizer using $\mathcal{D}_2^{\text{tr}}$, yielding the problem $\min_{\theta \in \Theta} \{ \mathcal{L}(\theta|\mathcal{D}_1^{\text{tr}}) + \lambda \cdot \mathcal{E}(\theta|\mathcal{D}_2^{\text{tr}}) \}$, where the cross-entropy loss is estimated using data set $\mathcal{D}_1^{\text{tr}}$.

C. Bayesian Learning

BNN training leverages *prior* knowledge on the *distribution* $p(\theta)$ of the model parameter vector θ , and it aims at finding a *distribution* $q(\theta)$ over the parameter vector θ that represents the learner's uncertainty in the model parameter space. The learning objective $\mathcal{F}(q|\mathcal{D}^{\text{tr}})$, known as *free energy*, accounts for the average loss $\mathbb{E}_{\theta \sim q(\theta)} [\mathcal{L}(\theta|\mathcal{D}^{\text{tr}})]$, as well for discrepancy between the distribution $q(\theta)$ and prior knowledge $p(\theta)$ as per the sum

$$\mathcal{F}(q|\mathcal{D}^{\text{tr}}) = \mathbb{E}_{\theta \sim q(\theta)} [\mathcal{L}(\theta|\mathcal{D}^{\text{tr}})] + \beta \cdot \text{KL}(q(\theta)||p(\theta)). \quad (11)$$

In (11), the discrepancy between distribution $q(\theta)$ and prior $p(\theta)$ is captured by the Kullback-Liebler (KL) divergence

$$\text{KL}(q(\theta)||p(\theta)) = \mathbb{E}_{q(\theta)} \left[\log \left(\frac{q(\theta)}{p(\theta)} \right) \right], \quad (12)$$

where we have introduced a hyperparameter $\beta > 0$. The KL term within free energy (11) reduces the calibration error by enforcing the adherence of the model parameter distribution $q(\theta)$ to the prior distribution $p(\theta)$.

Accordingly, BNN learning yields the optimized distribution $q^{\text{BNN}}(\theta)$ by addressing the minimization of the free energy as per

$$q^{\text{BNN}}(\theta) = \arg \min_{q(\theta)} \mathcal{F}(q|\mathcal{D}^{\text{tr}}), \quad (13)$$

and the corresponding trained probabilistic predictor is obtained as the *ensemble* [14]

$$p(y|x, \mathcal{D}^{\text{tr}}) = \mathbb{E}_{\theta \sim q^{\text{BNN}}(\theta)} [p(y|x, \theta)]. \quad (14)$$

Accordingly, the predictive probability distribution (14) requires averaging the output distribution $p(y|x, \theta)$ over the model parameter vector θ sampled from the distribution $q^{\text{BNN}}(\theta)$.

In practice, the optimization (13) over distribution $q(\theta)$ is often carried out over a parameterized class of distribution via *variational inference* (VI) [43], [44] (see [14, Ch. 12] for an overview). Specifically, denoting as $q(\theta|\varphi)$ a distribution over parameter vector θ parameterized by a vector φ , the problem (13) is simplified as

$$\varphi^{\text{BNN}} = \arg \min_{q(\theta|\varphi)} \mathcal{F}(q|\mathcal{D}^{\text{tr}}), \quad (15)$$

yielding the optimized variational distribution $q^{\text{BNN}}(\theta) = q(\theta|\varphi^{\text{BNN}})$. The parameter vector θ is typically assumed to follow a Gaussian distribution, with mean μ and covariance K included in the variational parameters as $\varphi = [\mu, K]$. Furthermore, the covariance K is often constrained to be diagonal with each i -th diagonal term modelled as $K_{ii} = \exp(\rho_i)$ for a learnable vector $\rho = [\rho_1, \dots, \rho_{n_p}]$, where n_p is the size of the model parameter vector θ . For a Gaussian variational distribution, problem (15) can be addressed via the reparametrization trick [45].

D. Calibration-Regularized Bayesian Learning

In the previous subsections, we have summarized existing ways to improve the ID calibration performance either via a calibration-based, data-dependent, regularizer (Sec. II-B) or via a prior-based, data-independent, regularizer (Sec. II-C). In this subsection, we first describe some limitations of the existing approaches as solutions to improve ID calibration, and then we propose the CBNN framework.

As described in Sec. II-B, CFNN training disregards epistemic uncertainty, i.e., uncertainty in the model parameter space, by optimizing over a single parameter vector θ^{CFNN} that minimizes a regularized training loss. This may cause the resulting CFNN predictor to remain over-confident on ID test inputs.

By capturing the epistemic uncertainty of the neural networks via ensembling as in (14), BNN learning has the potential to yield a better ID-calibrated probabilistic predictor that accounts for model-level uncertainty. However, in practice, BNNs may still yield poorly calibrated predictors in the presence of *model misspecification* [15]–[17], as well as due to *approximations* such as the

parametrization assumed by VI motivated by computational limitations. Model misspecification may refer to settings with a misspecified prior and/or to a misspecified likelihood $p(y|x, \theta)$, which do not reflect well the true data-generating distribution.

In order to handle the limitations of both CFNN and BNN, we propose CBNN. To this end, we first extend the calibration-based regularizer $\mathcal{E}(\theta|\mathcal{D}^{\text{tr}})$, defined in (8) for a deterministic model parameter vector θ , to a random vector $\theta \sim q(\theta)$ as

$$\mathcal{E}(q|\mathcal{D}^{\text{tr}}) = \mathbb{E}_{\theta \sim q(\theta)} [\mathcal{E}(\theta|\mathcal{D}^{\text{tr}})]. \quad (16)$$

The key idea underlying CBNN is to leverage the calibration regularizer (16) as a way to correct for the ID calibration errors arising from model misspecification and approximate Bayesian inference. Accordingly, adopting VI, CBNN learning aims at finding a variational parameter φ by addressing the minimization

$$\varphi^{\text{CBNN}} = \arg \min_{q(\theta|\varphi)} \{ \mathcal{F}(q|\mathcal{D}^{\text{tr}}) + \lambda \cdot \mathcal{E}(q|\mathcal{D}^{\text{tr}}) \}, \quad (17)$$

for some hyperparameter $\lambda > 0$. In practice, the optimization in (17) can be carried out via stochastic gradient descent (SGD) on the variational parameter φ via the reparameterization trick, in a manner similar to BNN learning (see Sec. II-C).

Finally, the trained probabilistic predictor is obtained as the ensemble

$$p(y|x, \mathcal{D}^{\text{tr}}) = \mathbb{E}_{\theta \sim q(\theta|\varphi^{\text{CBNN}})} [p(y|x, \theta)]. \quad (18)$$

As anticipated, as compared to existing schemes, CBNNs have two potential advantages. On the one hand, they can improve the calibration performance of CFNNs by taking epistemic uncertainty into account via the use of a variational distribution $q(\theta|\varphi)$ on the model parameter space. On the other hand, they can improve the calibration performance of BNN in the presence of model misspecification and/or approximation errors by modifying the free-energy loss function (15) through a calibration-driven regularizer. A summary of CBNN with a comparison to FNN, CFNN, and BNN is illustrated in Fig. 3.

III. BAYESIAN LEARNING WITH OOD CONFIDENCE MINIMIZATION

In the previous section, we have designed the CBNN training methodology with the aim at improving ID calibration performance. As discussed in Sec. I, another important requirement of reliable models is *OOD detection* [27], [46], i.e., the ability to distinguish OOD data from ID data. In this section, we describe an extension of CBNN that aims at improving the OOD

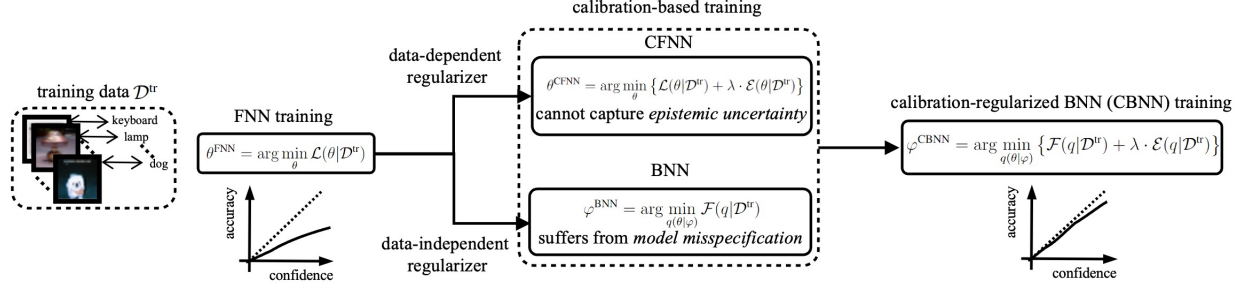


Fig. 3. Standard FNN training [14] minimizes the cross-entropy loss $\mathcal{L}(\theta|\mathcal{D}^{\text{tr}})$; CFNN training [22] minimizes the regularized cross-entropy loss (9); and BNN learning optimizes the free-energy loss in (11) [14]. The proposed CBNN optimizes a regularized free-energy loss with the aim of capturing epistemic uncertainty, like BNNs, while also accounting directly for calibration performance as CFNNs.

detection performance via the introduction of OCM [23]. To this end, we first describe the OOD detection problem; and then, we review the OCM regularizer presented in [23] to improve OOD detection for FNNs. Finally, we propose the inclusion of an OCM regularizer within the training process of CBNNs, defining the proposed CBNN-OCM scheme (see Fig. 1(c)).

A. OOD Detection

An important facet of calibration is the capacity of a model to detect OOD inputs, that is, inputs that suffer from a distributional shift with respect to training conditions [27]. OOD detection aims at distinguishing OOD inputs from ID inputs by relying on the observation of the confidence levels $p(y|x, \mathcal{D}^{\text{tr}})$ produced by the model [23], [47], [48]. The underlying principle is that, if the predictor $p(y|x, \mathcal{D}^{\text{tr}})$ is well calibrated, OOD inputs should be characterized by a high level of predictive uncertainty, i.e., by a higher-entropy conditional distribution $p(y|x, \mathcal{D}^{\text{tr}})$, as compared to ID inputs.

To quantify the effectiveness of OOD detection, one can thus use the discrepancy between the typical confidence levels $r(x) = p(\hat{y}(x)|x, \mathcal{D}^{\text{tr}})$ in (2) assigned to the hard decision $\hat{y}(x)$ in (1) for ID inputs and the typical confidence levels $r(x) = p(\hat{y}(x)|x, \mathcal{D}^{\text{tr}})$ for OOD inputs x . Indeed, if the confidence level $r(x)$ tends to be different for ID and OOD inputs, then OOD detection is likely to be successful.

To elaborate, we define $p^{\text{ID}}(r)$ as the distribution of the confidence levels $r(x)$ when x is an ID input, and $p^{\text{OOD}}(r)$ as the distribution of the confidence levels $r(x)$ when x is an OOD input.

Then, using standard results on the optimal probability of error for binary detection (see, e.g., [49]), one can use the *total variation* (TV) distance

$$\text{TV} = \int_0^1 |p^{\text{ID}}(r) - p^{\text{OOD}}(r)| dr \quad (19)$$

as a performance measure for OOD detection. In fact, when ID and OOD data are equally likely, the *optimal OOD detection probability* is given by

$$p_d^{\text{OOD}} = \frac{1}{2}(1 + \text{TV}). \quad (20)$$

B. OOD Confidence Minimization

In this subsection, we summarize OCM [23], state-of-the-art frequentist learning strategy, which improves the OOD detection performance of FNNs by leveraging an *unlabelled* OOD data set $\mathcal{D}^u = \{x^u[i]\}_{i=1}^{|\mathcal{D}^u|}$. The data set \mathcal{D}^u contains $|\mathcal{D}^u|$ inputs $x^u[i]$ that are generated from the marginal OOD input distribution $p_{\text{OOD}}(x)$ [12], [48]. Following [23], the unlabelled data set \mathcal{D}^u is referred to as the *uncertainty data set*.

Equipped with the uncertainty data set $\mathcal{D}^u = \{x^u[i]\}_{i=1}^{|\mathcal{D}^u|}$, OCM aims at *maximizing* the uncertainty of the predictor when applied to inputs in \mathcal{D}^u . This is done by considering a fictitious labelled data set in which all inputs $x^u[i]$ appear with all possible labels in set \mathcal{Y} . Accordingly, FNN training with OCM, referred to as FNN-OCM, addresses the problem

$$\theta^{\text{FNN-OCM}} = \arg \min_{\theta} \{ \mathcal{L}(\theta | \mathcal{D}^{\text{tr}}) + \gamma \cdot \mathcal{C}(\theta | \mathcal{D}^u) \}, \quad (21)$$

where the *OCM regularization* term is defined as the log-likelihood of the fictitious labelled data set, i.e.,

$$\mathcal{C}(\theta | \mathcal{D}^u) = - \sum_{i=1}^{|\mathcal{D}^u|} \sum_{y \in \mathcal{Y}} \log p(y | x^u[i], \theta), \quad (22)$$

given some hyperparameter $\gamma > 0$. It was shown in [23] that fine-tuning the pre-trained frequentist model $p(y|x, \theta^{\text{FNN}})$, with θ^{FNN} in (7), by solving problem (21) can significantly aid the OOD detection task. With the obtained solution, the trained probabilistic predictor for FNNs with OCM is obtained as

$$p(y|x, \mathcal{D}^{\text{tr}}) = p(y|x, \theta^{\text{FNN-OCM}}). \quad (23)$$

C. Calibration-Regularized Bayesian Learning with OOD Confidence Minimization

Even though FNN-OCM can help separating ID and OOD inputs, it inherits the poor ID calibration performance of FNNs, as it is unable to capture epistemic uncertainty. In contrast, BNNs and CBNNs can enhance ID calibration, while often failing at the OOD detection task due to computational limitations and model misspecification [2], [20], [21]. In order to enhance OOD detection, while still benefiting from the advantages of CBNN in ID calibration, in this subsection, we introduce CBNN-OCM by integrating CBNN and OCM.

To this end, we first generalize the OCM regularizer (22) so that it can be applied to a random model parameter vector $\theta \sim q(\theta)$ as the average

$$\mathcal{C}(q|\mathcal{D}^u) = \mathbb{E}_{\theta \sim q(\theta)} [\mathcal{C}(\theta|\mathcal{D}^u)] = -\mathbb{E}_{\theta \sim q(\theta)} \left[\sum_{i=1}^{|\mathcal{D}^u|} \sum_{y \in \mathcal{Y}} \log p(y|x^u[i], \theta) \right]. \quad (24)$$

Then, with (24), we propose to modify the objective of CBNN in (17) by adding the OCM regularizer as

$$\varphi^{\text{CBNN-OCM}}(\theta) = \arg \min_{q(\theta|\varphi)} \{ \mathcal{F}(q|\mathcal{D}^{\text{tr}}) + \lambda \cdot \mathcal{E}(q|\mathcal{D}^{\text{tr}}) + \gamma \cdot \mathcal{C}(q|\mathcal{D}^u) \}. \quad (25)$$

Finally, the trained probabilistic predictor is implemented as the ensemble

$$p(y|x, \mathcal{D}^{\text{tr}}) = \mathbb{E}_{\theta \sim q(\theta|\varphi^{\text{CBNN-OCM}})} [p(y|x, \theta)]. \quad (26)$$

With the introduction of both data-dependent and data-independent regularizers in (25), CBNN-OCM has the potential to provide reliable ID predictions, while also facilitating the detection of OOD inputs. A summary of the relation between FNN-OCM and CBNN-OCM is illustrated in Fig. 4.

IV. BAYESIAN LEARNING WITH SELECTIVE CALIBRATION

While CBNN-OCM is beneficial for OOD detection, it may potentially deteriorate the ID calibration performance of CBNN by modifying the operation of the model on examples that are hard to identify as ID or OOD. In this section, we introduce *selective calibration* as a way to correct this potential deterioration in ID performance. Selective calibration endows the model with the capacity to reject examples for which the gap between confidence and accuracy is expected to be excessive [24].

Like conventional selective classification [32], selective calibration adds the option for a model to refuse to produce a decision for some inputs. However, conventional selective classification

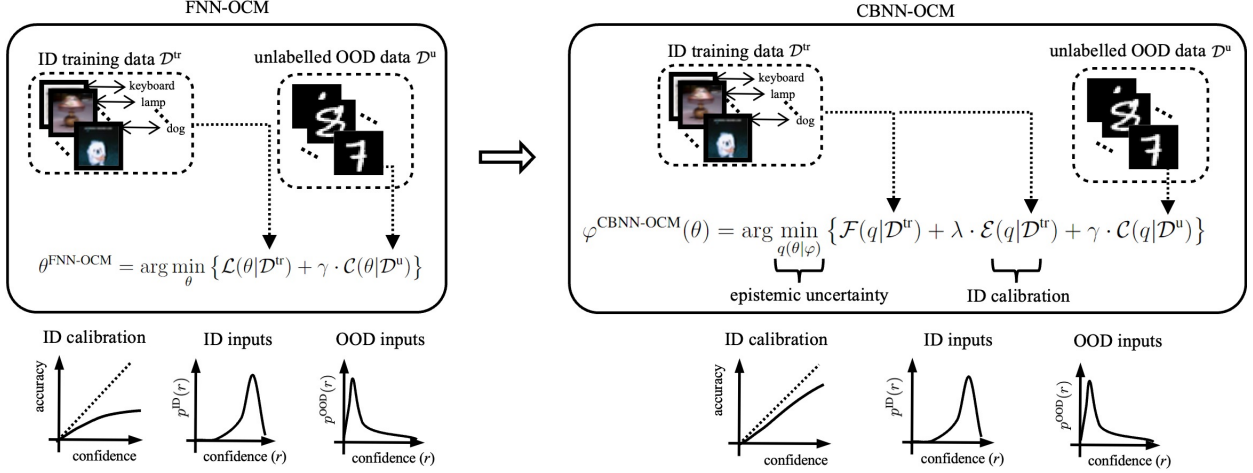


Fig. 4. Unlike standard FNNs that aim at maximizing the accuracy on the ID training data set, FNN-OCM (left) caters to the OOD detection task by maximizing the uncertainty for an unlabelled data set that contains OOD inputs. As a result, the model tends to assign different confidence levels $r(x) = p(\hat{y}(x)|x, \mathcal{D}^{tr})$ to ID and OOD inputs. The proposed CBNN-OCM (right) accounts for both ID calibration and OOD detection by capturing epistemic uncertainty as well as OOD uncertainty.

aims at rejecting examples with expected low accuracy. Accordingly, in order to ensure the successful selection of low-accuracy examples, selective classification requires the underlying model to be well calibrated, though possibly inaccurate. In contrast, selective calibration accepts examples with both high and low confidence levels, as long as the selector deems the confidence level to be close to the true accuracy. As a result, selective calibration does not require the underlying model to be well calibrated. Rather, it aims at enhancing calibration on the selected examples by making decisions only on inputs for which the model is expected to be well calibrated.

In this section, we first give a brief introduction to selective classification; then, we describe the selective calibration framework proposed in [24] for FNNs; and finally we present the SCBNN-OCM framework that combines selective calibration and CBNN-OCM (see Fig. 1(d)).

A. Selective Classification

Given a *pre-trained* model $p(y|x, \mathcal{D}^{tr})$, conventional selective classification optimizes a *selector* network $g(x|\phi) \in \{0, 1\}$ parameterized by a vector ϕ . An input is accepted if the selector outputs $g(x|\phi) = 1$, and is rejected if $g(x|\phi) = 0$.

To design the selector, assume that we have access to a held-out *validation data set* $\mathcal{D}^{\text{val}} = \{(x_i^{\text{val}}, y_i^{\text{val}})\}_{i=1}^{|\mathcal{D}^{\text{val}}|}$. Given a selector $g(x|\phi)$, the number of accepted examples is $\sum_{x \in \mathcal{D}^{\text{val}}} g(x|\phi)$. The *selector validation loss* is the loss evaluated only on the accepted samples of data set \mathcal{D}^{val} , i.e.,

$$\mathcal{R}(\phi|\mathcal{D}^{\text{val}}) = -\frac{\sum_{(x,y) \in \mathcal{D}^{\text{val}}} g(x|\phi) \cdot \log p(y|x, \mathcal{D}^{\text{tr}})}{\sum_{(x,y) \in \mathcal{D}^{\text{val}}} g(x|\phi)}. \quad (27)$$

The optimization of the selector network is formulated in [32] as the minimization of the selective validation loss (27) subject to a target coverage rate ξ , with $0 \leq \xi \leq 1$, i.e.,

$$\phi^{\text{S-Cla}} = \arg \min_{\phi} \mathcal{R}(\phi|\mathcal{D}^{\text{val}}) \quad \text{s.t.} \quad \frac{1}{|\mathcal{D}^{\text{val}}|} \sum_{x \in \mathcal{D}^{\text{val}}} g(x|\phi) \geq \xi. \quad (28)$$

By adopting the design criterion (27), selective classification aims at choosing only the inputs x for pairs (x, y) with large confidence levels $p(y|x, \mathcal{D}^{\text{tr}})$. As anticipated, this objective is sensible if the underlying model $p(y|x, \mathcal{D}^{\text{tr}})$ is sufficiently well calibrated. Reference [32] addressed the constrained optimization in (28) by converting it into an unconstrained problem via a quadratic penalty function (see [32, Eq. (2)]).

B. Selective Calibration

Like selective classification, given a pre-trained FNN model $p(y|x, \theta^{\text{FNN}})$, *selective calibration* introduces a selector network $g(x|\phi)$ that reject or accept an input x by setting $g(x|\phi) = 0$ or $g(x|\phi) = 1$, respectively. However, rather than targeting high-accuracy examples, selective calibration aims at accepting inputs x for which the confidence level $r(x) = p(\hat{y}(x)|x, \theta^{\text{FNN}})$ is expected to match the true accuracy of the hard decision $\hat{y}(x)$. Accordingly, the goal of the selector is to ensure the calibration condition (3) when conditioning on the accepted examples. The resulting *perfect selective ID calibration* condition can be formalized as

$$\Pr [y = \hat{y} | p(\hat{y}(x)|x, \theta^{\text{FNN}}) = r, g(x|\phi) = 1] = r, \quad \text{for all } r \in [0, 1]. \quad (29)$$

The condition (29) is less strict than the perfect ID calibration condition (3), since it is limited to accepted inputs.

1) *Training the Selector*: Generalizing the MMCE in (8), the ECE corresponding to the calibration criterion (29) can be estimated by using the accepted examples within the validation data set. This yields the *selective MMCE*

$$\mathcal{E}^{\text{S-Cal}}(\phi|\mathcal{D}^{\text{val}}) = \left(\frac{\sum_{i=1}^{|\mathcal{D}^{\text{val}}|} \sum_{j=1}^{|\mathcal{D}^{\text{val}}|} (c_i - r_i)(c_j - r_j) g(x_i^{\text{val}}|\phi) g(x_j^{\text{val}}|\phi) \kappa(r_i, r_j)}{\sum_{i=1}^{|\mathcal{D}^{\text{val}}|} \sum_{j=1}^{|\mathcal{D}^{\text{val}}|} g(x_i^{\text{val}}|\phi) g(x_j^{\text{val}}|\phi)} \right)^{\frac{1}{2}}, \quad (30)$$

with confidence scores $r_i = p(\hat{y}_i^{\text{val}}(x_i^{\text{val}})|x_i^{\text{val}}, \theta^{\text{FNN}})$ and correctness scores $c_i = \mathbb{1}(\hat{y}_i^{\text{val}}(x_i^{\text{val}}) = y_i^{\text{val}})$. Note that the selective MMCE recovers to the MMCE (8) when the selector accepts all examples, i.e., when $g(x|\phi) = 1$ for all inputs x . The parameter vector ϕ of the selector is obtained by optimizing the selective MMCE (30) by considering the targeted coverage rate constraint ξ , with $0 \leq \xi \leq 1$, as

$$\phi^{\text{S-Cal}} = \arg \min_{\phi} \mathcal{E}^{\text{S-Cal}}(\phi|\mathcal{D}^{\text{val}}) \quad \text{s.t.} \quad \frac{1}{|\mathcal{D}^{\text{val}}|} \sum_{x \in \mathcal{D}^{\text{val}}} g(x|\phi) \geq \xi. \quad (31)$$

Reference [24] addressed the constrained optimization in (31) by turning it into an unconstrained problem via the introduction of regularizer that accounts for the fraction of selected examples. To this end, the discrete-output function $g(x|\phi)$ is relaxed via a continuous-output function $\tilde{g}(r(x|\theta^{\text{FNN}}), s(x|\theta^{\text{FNN}})|\phi)$ that takes values within the interval $[0,1]$. The function $\tilde{g}(r(x|\theta^{\text{FNN}}), s(x|\theta^{\text{FNN}})|\phi)$ takes the confidence score

$$r(x|\theta^{\text{FNN}}) = p(\hat{y}(x)|x, \theta^{\text{FNN}}) \quad (32)$$

as input, as well as the *non-parametric outlier score vector* $s(x|\theta^{\text{FNN}})$ which will be specified shortly. All in all, problem (31) is approximately addressed by solving the problem

$$\phi^{\text{S-Cal}} = \arg \min_{\phi} \left\{ \tilde{\mathcal{E}}^{\text{S-Cal}}(\phi|\mathcal{D}^{\text{val}}) - \eta \cdot \sum_{x \in \mathcal{D}^{\text{val}}} \log(\tilde{g}(r(x|\theta^{\text{FNN}}), s(x|\theta^{\text{FNN}})|\phi)) \right\}, \quad (33)$$

where

$$\tilde{\mathcal{E}}^{\text{S-Cal}}(\phi|\mathcal{D}^{\text{val}}) = \left(\sum_{i=1}^{|\mathcal{D}^{\text{val}}|} \sum_{j=1}^{|\mathcal{D}^{\text{val}}|} (c_i - r_i)(c_j - r_j) \tilde{g}(r_i, s_i|\phi) \tilde{g}(r_j, s_j|\phi) \kappa(r_i, r_j) \right)^{\frac{1}{2}}, \quad (34)$$

with confidence score $r_i = r(x_i^{\text{val}}|\theta^{\text{FNN}})$ and non-parametric outlier score vector $s_i = s(x_i^{\text{val}}|\theta^{\text{FNN}})$, and $\eta \geq 0$ is a coefficient that balances selective calibration performance and coverage. Note that function (34) is the numerator of (30) with the relaxed selector $\tilde{g}(r(x|\theta^{\text{FNN}}), s(x|\theta^{\text{FNN}})|\phi)$ in lieu of $g(x|\phi)$, and that $-\log(\cdot)$ plays the role of a barrier function to enforce the coverage rate constraint [50].

2) *Non-Parametric Outlier Score Vector*: The non-parametric outlier score vector $s(x|\theta^{\text{FNN}})$ of an input x has the goal of quantifying the extent to which input x conforms with the input in the training data set $\mathcal{X}^{\text{tr}} = \{x_i\}_{i=1}^{|\mathcal{D}^{\text{tr}}|}$. The rationale for adding $s(x|\theta^{\text{FNN}})$ as an input to the selector is that inputs x that are too “far” from the training set may yield more poorly calibrated decisions by the model $p(y|x, \theta^{\text{FNN}})$. The authors of [24] included four different features in vector $s(x|\theta^{\text{FNN}})$, which are obtained from a kernel density estimator, an isolation forest, a one-class

support vector machine, and a k -nearest neighbor distance, constructing a 4×1 score vector $s(x|\theta^{\text{FNN}})$. In particular, the first element of vector $s(x|\theta^{\text{FNN}})$ is obtained by the kernel density estimator [51]

$$s_1(x|\theta^{\text{FNN}}) = \frac{1}{|\mathcal{X}^{\text{tr}}|} \sum_{i=1}^{|\mathcal{X}^{\text{tr}}|} \kappa(\|z - z_i^{\text{tr}}\|), \quad (35)$$

where $\kappa(\cdot)$ is a kernel function; z is the output of the last hidden layer of the parametrized network $p(y|x, \theta^{\text{FNN}})$; and, similarly, z_i^{tr} is the corresponding feature vector for $p(y|x_i, \theta^{\text{FNN}})$. Details regarding the other elements of the score vector $s(x|\theta^{\text{FNN}})$ can be found in Appendix A.

3) *Inference with the Selector*: During testing, the binary selector $g(x|\phi^{\text{S-Cal}})$ is obtained via thresholding as

$$g(x|\phi^{\text{S-Cal}}) = \mathbb{1}(\tilde{g}(r(x|\theta^{\text{FNN}}), s(x|\theta^{\text{FNN}})|\phi^{\text{S-Cal}}) \geq \tau), \quad (36)$$

where τ is a hyperparameter controlling the fraction of selected examples. In this regard, we note that the targeted coverage rate ξ can be in principle met by changing only the hyperparameter η in (33) without requiring the choice of the threshold τ in (36). However, this would require retraining of the selector any time the desired coverage level ξ is changed. Hence, reference [24] introduced the additional hyperparameter τ that can adjust the coverage given a fixed, trained, selector $\phi^{\text{S-Cal}}$.

C. Bayesian Learning with Selective Calibration

In order to extend selective calibration to CBNN-OCM, we propose to apply the selective MMCE criterion in (30) with confidence score and outlier score vector averaged over the model distribution $q(\theta|\varphi^{\text{CBNN-OCM}})$ in (25). Specifically, the average confidence score $\bar{r}(x|\varphi^{\text{CBNN-OCM}})$ is defined as

$$\bar{r}(x|\varphi^{\text{CBNN-OCM}}) = \max_{y' \in \mathcal{Y}} \mathbb{E}_{\theta \sim q(\theta|\varphi^{\text{CBNN-OCM}})} [p(y'|x, \theta)], \quad (37)$$

and the average non-parametric outlier score vector is given by

$$\bar{s}(x|\varphi^{\text{CBNN-OCM}}) = \mathbb{E}_{\theta \sim q(\theta|\varphi^{\text{CBNN-OCM}})} [s(x|\theta)], \quad (38)$$

with vector $s(x|\theta)$ defined as in the previous subsection.

With these definitions, the selector parameter vector $\phi^{\text{SCBNN-OCM}}$ is obtained by addressing the problem

$$\phi^{\text{SCBNN-OCM}} = \arg \min_{\phi} \left\{ \tilde{\mathcal{E}}^{\text{S-Cal}}(\phi|\mathcal{D}^{\text{val}}) - \eta \cdot \sum_{x \in \mathcal{D}^{\text{val}}} \log \tilde{g}(\bar{r}(x|\varphi^{\text{CBNN-OCM}}), \bar{s}(x|\varphi^{\text{CBNN-OCM}})|\phi) \right\}, \quad (39)$$

where

$$\tilde{\mathcal{E}}^{\text{S-Cal}}(\phi|\mathcal{D}^{\text{val}}) = \left(\sum_{i=1}^{|\mathcal{D}^{\text{val}}|} \sum_{j=1}^{|\mathcal{D}^{\text{val}}|} (c_i - \bar{r}_i)(c_j - \bar{r}_j) \tilde{g}(\bar{r}_i, \bar{s}_i|\phi) \tilde{g}(\bar{r}_j, \bar{s}_j|\phi) \kappa(\bar{r}_i, \bar{r}_j) \right)^{\frac{1}{2}}, \quad (40)$$

with average confidence score $\bar{r}_i = \bar{r}(x_i^{\text{val}}|\varphi^{\text{CBNN-OCM}})$ and average non-parametric outlier score vector $\bar{s}_i = \bar{s}(x_i^{\text{val}}|\varphi^{\text{CBNN-OCM}})$.

Finally, during inference, the binary selector $g(x|\phi^{\text{SCBNN-OCM}})$ is obtained via the thresholding in a manner similar to (36), i.e.,

$$g(x|\phi^{\text{SCBNN-OCM}}) = \mathbb{1} \left(\tilde{g}(\bar{r}(x|\varphi^{\text{CBNN-OCM}}), \bar{s}(x|\varphi^{\text{CBNN-OCM}})|\phi^{\text{SCBNN-OCM}}) \geq \tau \right), \quad (41)$$

for some threshold τ . A summary of SCBNN-OCM is illustrated in Fig. 5.

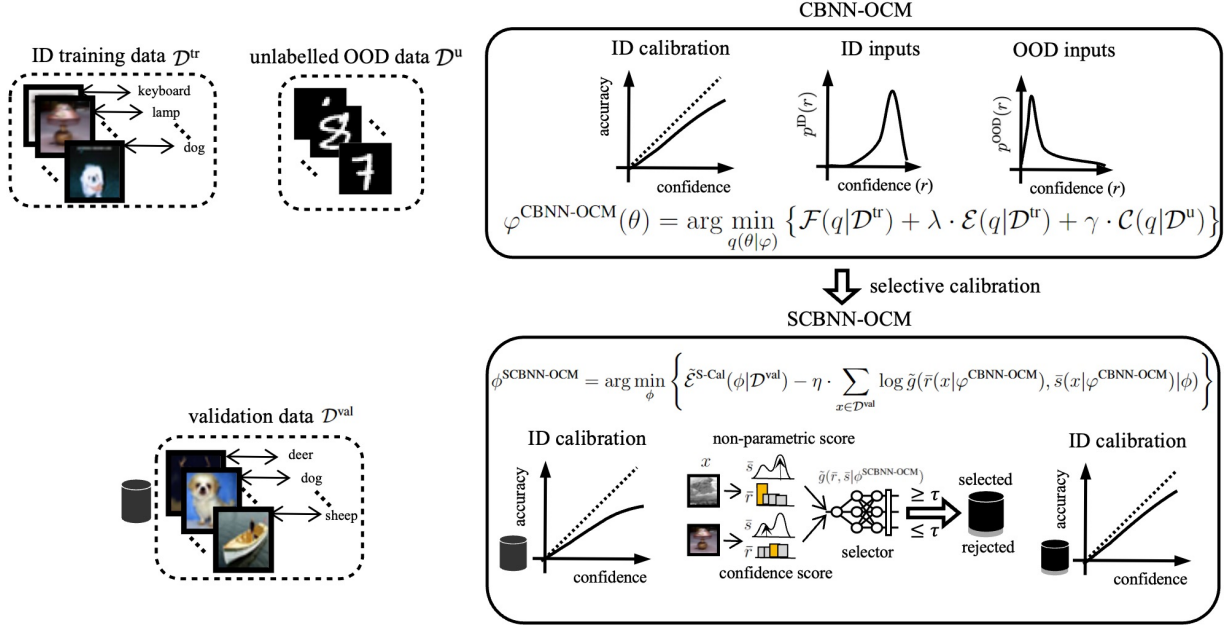


Fig. 5. Given a fixed, pre-trained model parameter vector $\theta \sim q(\theta|\varphi^{\text{CBNN-OCM}})$, selective calibration aims at achieving well-calibrated decisions (3) on the selected inputs (hence aiming at (29)) by rejecting inputs on which the discrepancy between confidence and accuracy is expected to be large.

V. EXPERIMENTS

In this section, we report on the effectiveness of calibration-based training, OCM, and selective calibration for frequentist and Bayesian learning in terms of ID and OOD calibration performance.

A. Setting and Metrics

All experiments use the CIFAR-100 data set [37] to generate ID samples and the TinyImageNet (resized) data set [38] to generate OOD samples [23]. The parameterized predictor $p(y|x, \theta)$ adopts the WideResNet-40-2 architecture [52], and the variational distribution $q(\theta|\varphi)$ is Gaussian with mean and diagonal covariance being the variational parameter φ . For the selective inference task, we use a 3-layer ReLU activated feed-forward neural network $g(x|\phi)$ with 64 dimensional hidden layer [24].

We consider the following evaluation criteria: (i) the *reliability diagram*, which plots accuracy against confidence as defined in Sec. II-A with number of bins $M = 15$ (we only visualize the bins that have number of samples no smaller than 100 to avoid undesired statistical noise [53], [54]); (ii) the *ECE*, which evaluates the average discrepancy between per-bin accuracy and per-bin confidence as defined in (6); (iii) *ID accuracy*, marked as “Acc”, which is the proportion of the ID data for which a correct prediction is made; (iv) *OOD detection probability*, which is the optimal probability of successfully detecting OOD data, as defined in (20); and (v) *ID coverage rate*, which is the fraction of selected data points on the ID test data set for selective calibration. We refer to Appendix C for all the experimental details¹.

B. Can Calibration-Regularization Enhance ID Calibration for Bayesian Learning?

We first evaluate the ID calibration performance for (i) FNN, defined as in (7); (ii) CFNN with calibration-based regularization [22], as defined in (9); (iii) BNN as per (13); and (iv) the proposed CBNN as per (17). To this end, we present reliability diagrams, as described in Sec. II, as well as the trade-off between accuracy and calibration obtained by varying the hyperparameter λ in the designed objectives (9) and (17).

To start, in Fig. 6, we show the reliability diagrams for all the four schemes, which are evaluated on the CIFAR-100 data set. Note that the figure also plots test accuracy, reported as “Acc”, and ECE. BNN is observed to yield better calibrated predictions than FNN with a slight improvement in accuracy, while calibration-based regularization improves the calibration performance for both FNN and BNN. In particular, the ECE is decreased by more than 20% for frequentist learning and by 50% for Bayesian learning.

¹Code can be found at <https://github.com/kclip/Calibrating-Bayesian-Learning>.

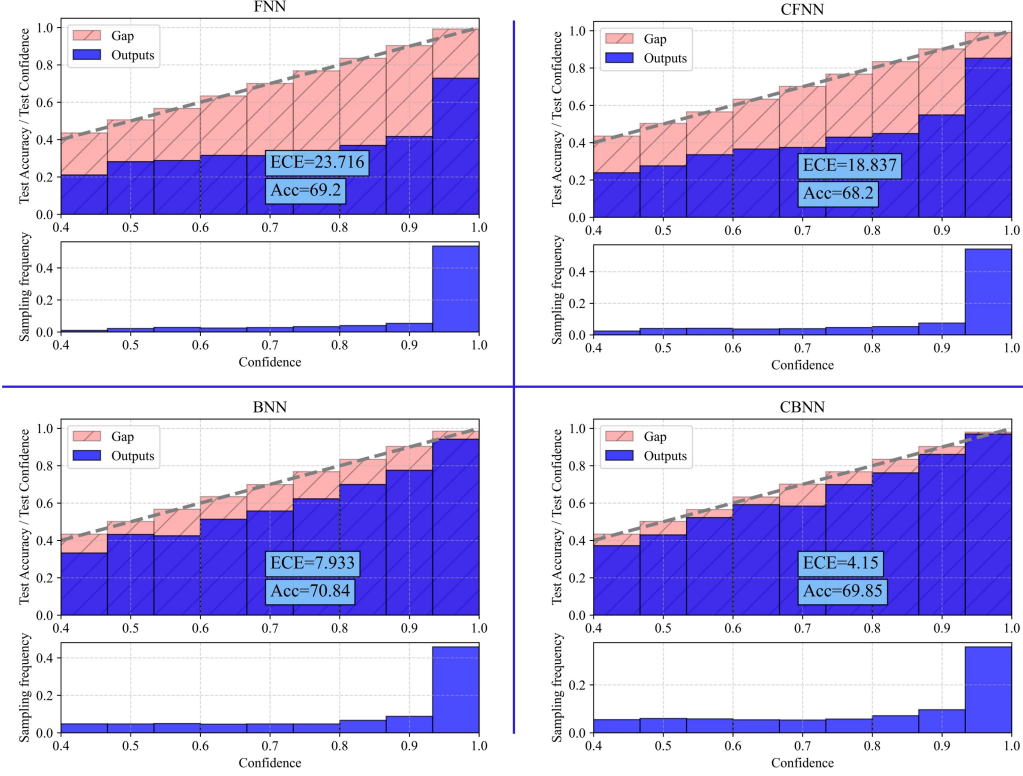


Fig. 6. Reliability diagrams for the CIFAR-100 classification task given the predictor trained using (i) FNN (top-left); (ii) CFNN (top-right); (iii) BNN (bottom-left); and (iv) CBNN (bottom-right).

Fig. 7 demonstrates the trade-off between accuracy and ECE obtained by varying the hyperparameter λ in (9) and (17). Note that with $\lambda = 0$, one recovers FNN and BNN from CFNN and CBNN, respectively. Increasing the value of λ is seen to decrease the ECE for both CFNN and CBNN and to gradually affect the accuracy, tracing a trade-off between ID calibration and accuracy. This figure also report on the OOD detection probability, which will be discussed later in this section.

C. Can Confidence Minimization Improve OOD Detection without Affecting ID Performance?

To evaluate the performance in terms of OOD detection, we select ID data from the CIFAR-100 data set, which is also used for training, while OOD is selected from the TinyImageNet data set. As a reference, the color map in Fig. 7 shows that the OOD detection probability (20) does not necessarily increase as the ID calibration performance improved, which is most notable for BNN. This highlights the importance of introducing mechanism tailored to enhancing OOD

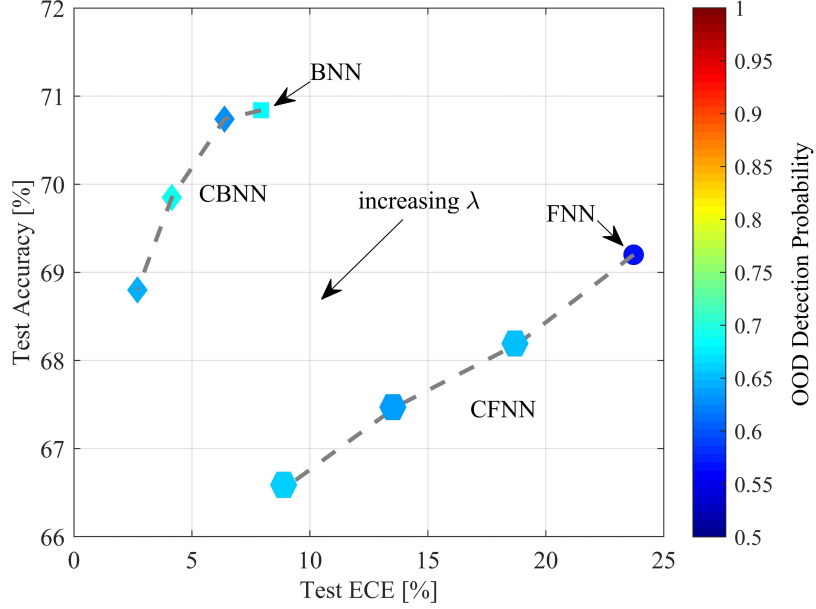


Fig. 7. Accuracy versus ECE obtained by changing the hyperparameter λ on CIFAR-100 data set for FNN, CFNN, BNN, and CBNN, with OOD detection probability indicated by the marker's color.

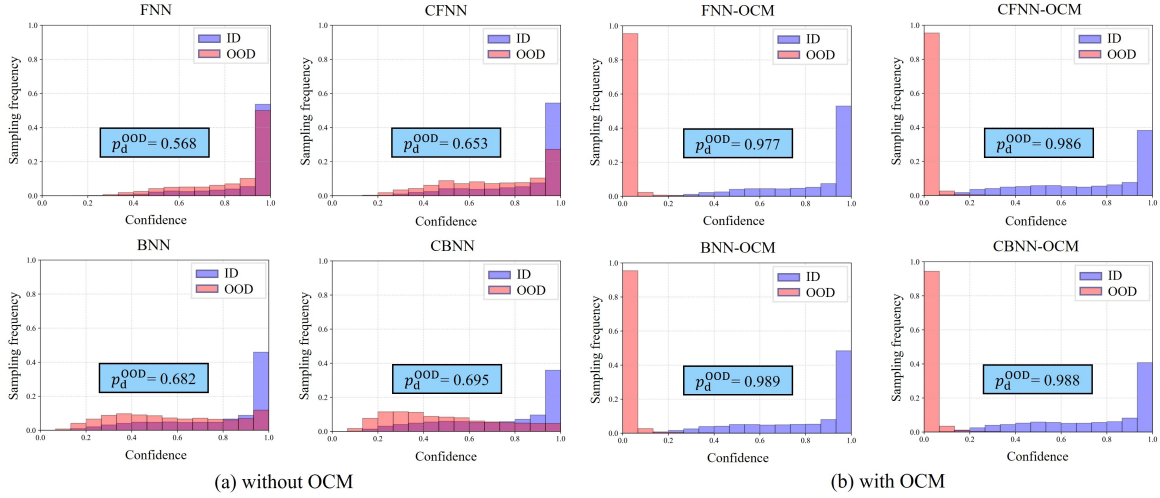


Fig. 8. Confidence histograms for ID and OOD data drawn from CIFAR-100 and TinyImageNet data sets, respectively, for FNN, CFNN, FNN-OCM, CFNN-OCM, BNN, CBNN, BNN-OCM, and CBNN-OCM, with hyperparameter $\gamma = 0.5$ [23].

detection performance, such as OCM.

To evaluate the benefits of OCM, Fig. 8 plots the histograms of the confidence levels produced by different models for ID and OOD data. The more distinct the two distributions are, the larger the OOD detection probability (20) is [23], [49]. First, it is observed that BNN can improve

OOD detection as compared to FNN, but the OOD confidence levels tend to be approximately uniformly distributed. Second, calibration-regularization, while improving ID calibration, does not help with OOD detection, as it focuses solely on ID performance. Finally, OCM can drastically enhance OOD detection performance for both FNN and BNN, with and without calibration-regularizers. In particular, thanks to OCM, the model produces low confidence levels on OOD inputs, enhancing the OOD detection probability (20).

To further investigate the interplay between ID and OOD performance, Fig. 9 plots the ID test accuracy versus the OOD detection probability by varying the hyperparameter γ in (21) and (25). BNN yields better test accuracy for any given OOD detection probability level, and adding calibration-regularizer improves ID calibration performance, but at the cost of a reduced ID accuracy for a given OOD detection probability level.

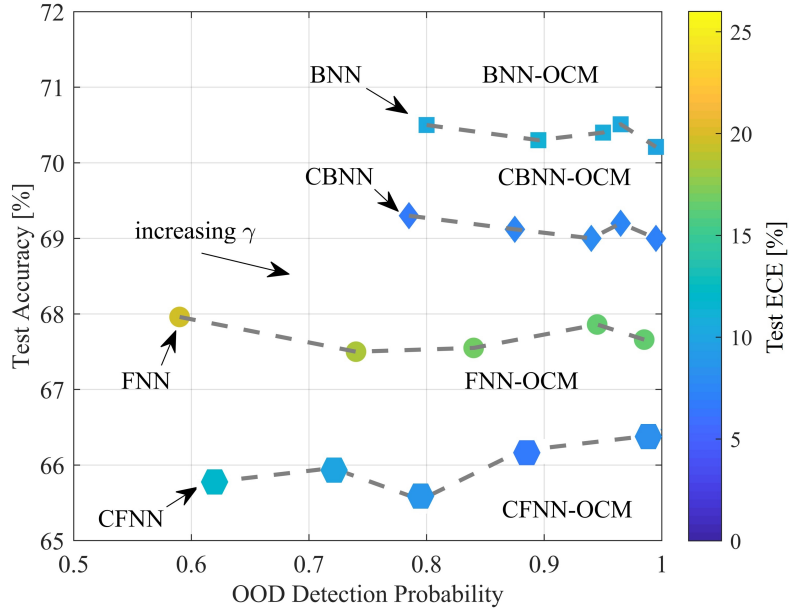


Fig. 9. Test accuracy versus OOD detection probability for FNN-OCM, CFNN-OCM, BNN-OCM, and CBNN-OCM, with test ECE as the marker's color. Note that hyperparameter $\gamma = 0$ recovers the original schemes without OCM regularizer.

D. Can Selective Calibration Compensate for the ID Performance Loss of OCM?

So far, we have seen that there is generally a trade-off between ID and OOD performance. In particular, from Fig. 9, it was concluded that, for a given fixed level of OOD detection probability,

calibration-regularized learning improved ID calibration at the cost of the ID accuracy for BNN-OCM. In this subsection, we ask whether selective calibration can ensure a synergistic use of OCM and calibration-aware regularization, guaranteeing that CBNN-OCM achieves the best ID and OOD performance levels. To address this question, we vary the ID coverage rate, i.e., the fraction of accepted ID samples, by changing the hyperparameter τ in (41). The resulting ID and OOD performance is shown in Fig. 10 for SBNN-OCM and SCBNN-OCM.

The figure demonstrates that, thanks to selective calibration, SCBNN-OCM outperforms SBNN-OCM in terms of all metrics, namely ID accuracy, ID calibration, and OOD detection probability, for a sufficiently low coverage rate, here around 50%. We thus conclude that, by selecting examples with sufficiently good ID calibration performance, SCBNN-OCM can fully benefit from calibration-aware regularization, enhancing ID performance, as well as from OCM, improving OOD detection performance. That said, the need to accept a sufficiently small number of inputs to ensure this result highlights the challenges of guaranteeing both ID and OOD performance levels.

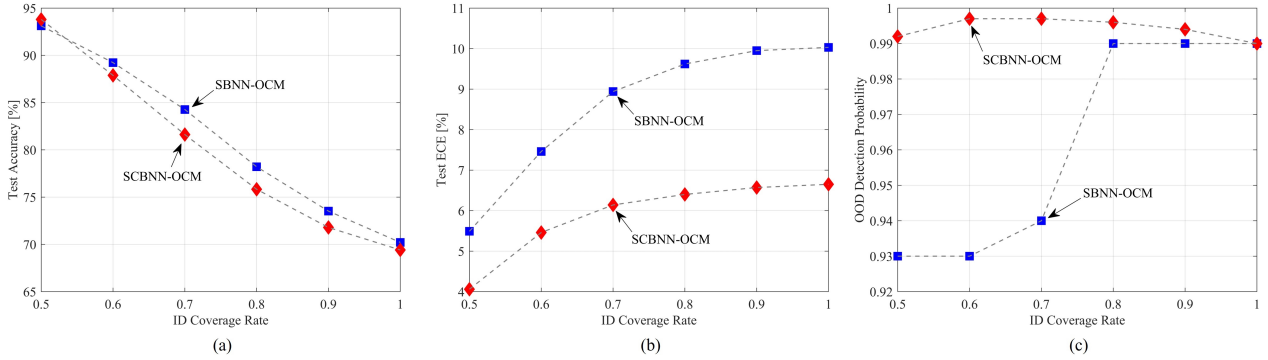


Fig. 10. Test accuracy, ECE, and OOD detection probability versus ID coverage rate for SBNN-OCM and SCBNN-OCM.

VI. CONCLUSION

In this paper, we have proposed SCBNN-OCM, a general framework that generalizes variational inference-based Bayesian learning to target both ID and OOD calibration. To improve ID calibration, we have introduced a regularizer based on the calibration error, while OOD calibration is enhanced by means of data augmentation based on confidence minimization. In order to facilitate the synergistic use of calibration-aware regularization and OCM regularization, we have finally introduced a selective calibration strategy that rejects examples that are likely

to have poor ID calibration performance. Numerical results have illustrated the challenges in ensuring both ID and OOD performance, as schemes designed for ID calibration may end up hurting OOD calibration, and vice versa. That said, thanks to selective calibration, SCBNN-OCM was observed to achieve the best ID and OOD performance as compared to the other benchmarks as long as one allows for a sufficiently large number of rejected samples. Interesting directions for future work include extending the proposed framework to likelihood-free, simulation-based inference [55], to continual learning [56], and to large language models [4].

APPENDIX

A. Non-Parametric Outlier Score Vectors

In this subsection, we specify the details for non-parametric outlier score vector $s(x|\theta^{\text{FNN}})$ described in Sec. IV-B2, which can be implemented by following the sklearn package in Python. As mentioned in the text, the first entry is given by (35) with the Gaussian kernel $\kappa(\|z - z_i^{\text{tr}}\|) = \exp(-\|z - z_i^{\text{tr}}\|^2/h)$ given the bandwidth parameter $h > 0$.

The isolation forest score for x , $s_2(x|\theta^{\text{FNN}})$, is obtained by evaluating the *depth* of z in the *isolation forest*, which is a collection of T binary trees in which each binary tree is constructed so that every element in $\{z_i^{\text{tr}}\}_{i=1}^{|\mathcal{X}^{\text{tr}}|} \cup \{z\}$ is assigned to a leaf node. Specifically, the isolation forest score is evaluated as [57]

$$s_2(x|\theta^{\text{FNN}}) = 2^{-\frac{\sum_{t=1}^T h_t(z)}{T \cdot c}}, \quad (42)$$

where $h_t(z)$ is the depth of z in the t -th binary tree given a normalization constant c .

The one-class support vector machine (SVM) score for x , $s_3(x|\theta^{\text{FNN}})$, can be expressed as [58]

$$s_3(x|\theta^{\text{FNN}}) = \sum_{i=1}^{|\mathcal{X}^{\text{tr}}|} \alpha_i \kappa(\|z - z_i^{\text{tr}}\|) - \rho, \quad (43)$$

in which the coefficients $\alpha_i \geq 0$ for $i = 1, \dots, |\mathcal{X}^{\text{tr}}|$, satisfying $\sum_{i=1}^{|\mathcal{X}^{\text{tr}}|} \alpha_i = 1$, are optimized along with the offset parameter $\rho \in \mathbb{R}$ in order to separate the training data $\{z_i^{\text{tr}}\}_{i=1}^{|\mathcal{X}^{\text{tr}}|}$ from the origin in the feature space associated with the kernel $\kappa(\cdot)$ [58, Sec. 5].

Finally, k -nearest neighbor distance for x , $s_4(x|\theta^{\text{FNN}})$, can be written as [59]

$$s_4(x|\theta^{\text{FNN}}) = \|z - z_i^{\text{tr}}\|_{(k)}, \quad (44)$$

where $\|z - z_i^{\text{tr}}\|_{(k)}$ is the k -th smallest value in the set of distances $\{\|z - z_i^{\text{tr}}\|\}_{i=1}^{|\mathcal{X}^{\text{tr}}|}$.

B. Algorithmic Tables

Details for SCBNN-OCM training process are in Algorithm 1, while the SCBNN-OCM inference process is summarized in Algorithm 2.

C. Experiment Details

In this subsection, we specify the implementation details for the experimental results in Sec. V. All the experiments are implemented by PyTorch [60] and ran over a GPU server with single NVIDIA A100 card.

1) Architecture and Training Details for Calibration-Regularized Learning:

Architecture: For all the experiments related to calibration-regularized learning, we adopt the WideResNet-40-2 architecture [52].

Hyperparameters: For fair comparison, we use the same training policy for both frequentist and Bayesian learning. Specifically, we use the SGD optimizer with momentum factor 0.9 and train the model during 100 epochs. We also decrease the learning rate by dividing its value by a factor of 5 for every 30 epochs with initial learning rate 0.1 in a manner similar to [23]. The minibatch size used for single SGD update is set to 128. For Bayesian learning, we set as prior $p(\theta)$ the Gaussian distribution that has zero-mean vector with diagonal covariance matrix having each element as 0.001. The hyperparameter β for the free energy (11) is set to 0.00035. The ensemble size R^{tr} for Bayesian learning during training (see Algorithm 1) is set to 1, while the ensemble size R^{te} during testing (see Algorithm 2) is set to 20. The hyperparameter of calibration-based regularizer λ in (9) and (17) is chosen as the value in set $\{0.2, 0.4, 0.6, 0.8, 1.0, 2.0, 3.0, \dots, 10.0\}$ that achieves the lowest ECE, while preserving the accuracy drop no larger than 1.5% as compared to the one without the calibration-based regularizer ($\lambda = 0$), in a manner similar to [28]. The corresponding accuracy and ECE are evaluated based on the validation data set \mathcal{D}^{val} , and the hyperparameter λ for FNN and λ for BNN are chosen independently, which result in the values of 3 and 0.8 respectively in our experiments. We use weighted MMCE regularizer for calibration-aware regularization term $\mathcal{E}(\theta|\mathcal{D}^{\text{tr}})$, which is defined as [22]

$$\mathcal{E}(\theta|\mathcal{D}^{\text{tr}}) = \left(\sum_{i,j:c_i=c_j=0} \frac{r_i r_j \kappa(r_i, r_j)}{(|\mathcal{D}^{\text{tr}}| - n_c)(|\mathcal{D}^{\text{tr}}| - n_c)} + \sum_{i,j:c_i=c_j=1} \frac{(1 - r_i)(1 - r_j) \kappa(r_i, r_j)}{n_c^2} - 2 \sum_{i,j:c_i=1, c_j=0} \frac{(1 - r_i) r_j \kappa(r_i, r_j)}{(|\mathcal{D}^{\text{tr}}| - n_c) n_c} \right)^{\frac{1}{2}}, \quad (45)$$

where the kernel function is $\kappa(r_i, r_j) = \exp(-||r_i - r_j||/0.4)$, and n_c is the number of correct examples, i.e., $n_c = \sum_{i=1}^{|\mathcal{D}^{\text{tr}}|} c_i$.

Data set split and augmentations: As mentioned in Sec. V-A, we choose CIFAR-100 data set [37] for the ID samples, which is a data set composed of 60,000 images each with label information chosen among 100 different classes. In particular, CIFAR-100 splits the data set into two parts: 50,000 for training and 10,000 for testing; and we further split the training data set into 45,000 examples and 5,000 examples to define the training data set \mathcal{D}^{tr} and the validation data set \mathcal{D}^{val} . We adopt the standard random flip and random crop augmentations provided by Pytorch [60] during the training process.

2) Architecture and Training Details for OOD Detection:

Architecture: Since we use the same predictor for OOD detection, the corresponding architecture remains the same, i.e., WideResNet-40-2, as described above.

Hyperparameters: Following the original OCM paper [23], OOD confidence minimization (21) and (25) is carried out by fine-tuning based on the corresponding pre-trained models, e.g., CBNN-OCM is obtained via fine-tuning with the OCM-regularized training loss given the pre-trained CBNN. Uncertainty data set \mathcal{D}^{u} is constructed by randomly choosing 6,000 input data from TinyImageNet. During fine-tuning, SGD optimizer with momentum factor of 0.9 is adopted during 10 epochs, each consisting 282 iterations. The initial learning rate is set to 0.001, and we update the learning rate for each iteration by following [61]. Specifically, during SGD training, for each epoch, we first sample 9,000 examples from \mathcal{D}^{tr} and evaluate the ID-related training measures for each SGD update via sampling 32 examples (minibatch size being 32) without replacement among the 9,000 examples; for the OOD-related training measures, we sample 64 examples (minibatch size being 64) among \mathcal{D}^{u} with replacement. Other hyperparameters are the same as calibration-regularized learning described in the previous subsection.

Data set split and augmentations: TinyImageNet data set [38] contains 10,000 images that corresponds to different 200 classes. We split the input data of TinyImageNet data set into two parts, 6,000 and 4,000, and use them for the uncertainty data set \mathcal{D}^{u} and for the OOD test data set, respectively. During fine-tuning, we apply the same standard random flip and random crop augmentations to both \mathcal{D}^{tr} and \mathcal{D}^{u} .

3) Architecture and Training Details for Selective Calibration:

Architecture: For the selector implementation, we use a 3-layer feed-forward neural network with 64 neurons in each hidden layer, activated by ReLU.

Hyperparameters: For selector training (33) and (39), we use Adam optimizer, with learning rate 0.001 and weight decay coefficient 10^{-5} . We train the model for 5 epochs, each epoch consisting 50,000 iterations, and each iteration samples 32 examples (minibatch size being 32) among \mathcal{D}^{val} . The hyperparameter η in (33) and (39) are set to 0.01, and we set the kernel function in (40) as $\kappa(r_i, r_j) = \exp(-||r_i - r_j||/0.2)$. We use the same R^{tr} and R^{te} as in calibration-regularized training (see Algorithm 1, 2).

Data set split and augmentations: As described above, \mathcal{D}^{val} has 5,000 examples obtained from CIFAR-100 data set. We utilize the standard random flip and random crop augmentations during selector training.

REFERENCES

- [1] S. Herbold, A. Hautli-Janisz, U. Heuer, Z. Kikteva, and A. Trautsch, “A large-scale comparison of human-written versus ChatGPT-generated essays,” *Scientific Reports*, vol. 13, no. 1, p. 18617, 2023.
- [2] Y. Ovadia, E. Fertig, J. Ren, Z. Nado, D. Sculley, S. Nowozin, J. Dillon, B. Lakshminarayanan, and J. Snoek, “Can you trust your model’s uncertainty? Evaluating predictive uncertainty under dataset shift,” *Advances in neural information processing systems*, vol. 32, 2019.
- [3] A. Esteva, B. Kuprel, R. A. Novoa, J. Ko, S. M. Swetter, H. M. Blau, and S. Thrun, “Dermatologist-level classification of skin cancer with deep neural networks,” *nature*, vol. 542, no. 7639, pp. 115–118, 2017.
- [4] G. Detommaso, M. Bertran, R. Fogliato, and A. Roth, “Multicalibration for confidence scoring in LLMs,” *arXiv preprint arXiv:2404.04689*, 2024.
- [5] B. Kumar, C. Lu, G. Gupta, A. Palepu, D. Bellamy, R. Raskar, and A. Beam, “Conformal prediction with large language models for multi-choice question answering,” *arXiv preprint arXiv:2305.18404*, 2023.
- [6] A. Shih, D. Sadigh, and S. Ermon, “Long horizon temperature scaling,” in *International Conference on Machine Learning*. PMLR, 2023, pp. 31 422–31 434.
- [7] V. Quach, A. Fisch, T. Schuster, A. Yala, J. H. Sohn, T. S. Jaakkola, and R. Barzilay, “Conformal language modeling,” *arXiv preprint arXiv:2306.10193*, 2023.
- [8] B. Rajendran, O. Simeone, and B. M. Al-Hashimi, “Towards efficient and trustworthy AI through hardware-algorithm-communication co-design,” *arXiv preprint arXiv:2309.15942*, 2023.
- [9] M. Zecchin, S. Park, and O. Simeone, “Forking uncertainties: Reliable prediction and model predictive control with sequence models via conformal risk control,” *IEEE Journal on Selected Areas in Information Theory*, 2024.
- [10] L. Lindemann, M. Cleaveland, G. Shim, and G. J. Pappas, “Safe planning in dynamic environments using conformal prediction,” *IEEE Robotics and Automation Letters*, 2023.
- [11] A. Z. Ren, A. Dixit, A. Bodrova, S. Singh, S. Tu, N. Brown, P. Xu, L. Takayama, F. Xia, J. Varley *et al.*, “Robots that ask for help: Uncertainty alignment for large language model planners,” *arXiv preprint arXiv:2307.01928*, 2023.

- [12] B. Lakshminarayanan, A. Pritzel, and C. Blundell, “Simple and scalable predictive uncertainty estimation using deep ensembles,” *Advances in neural information processing systems*, vol. 30, 2017.
- [13] R. Krishnan and O. Tickoo, “Improving model calibration with accuracy versus uncertainty optimization,” *Advances in Neural Information Processing Systems*, vol. 33, pp. 18 237–18 248, 2020.
- [14] O. Simeone, *Machine learning for engineers*. Cambridge university press, 2022.
- [15] A. Masegosa, “Learning under model misspecification: Applications to variational and ensemble methods,” *Advances in Neural Information Processing Systems*, vol. 33, pp. 5479–5491, 2020.
- [16] W. R. Morningstar, A. Alemi, and J. V. Dillon, “ PAC^m -Bayes: Narrowing the empirical risk gap in the misspecified Bayesian regime,” in *International Conference on Artificial Intelligence and Statistics*. PMLR, 2022, pp. 8270–8298.
- [17] M. Zecchin, S. Park, O. Simeone, M. Kountouris, and D. Gesbert, “Robust PAC^m : Training ensemble models under misspecification and outliers,” *IEEE Transactions on Neural Networks and Learning Systems*, 2023.
- [18] J. Knoblauch, J. Jewson, and T. Damoulas, “Generalized variational inference: Three arguments for deriving new posteriors,” *arXiv preprint arXiv:1904.02063*, 2019.
- [19] F. Wenzel, K. Roth, B. S. Veeling, J. Światkowski, L. Tran, S. Mandt, J. Snoek, T. Salimans, R. Jenatton, and S. Nowozin, “How good is the Bayes posterior in deep neural networks really?” *arXiv preprint arXiv:2002.02405*, 2020.
- [20] Y. Wald, A. Feder, D. Greenfeld, and U. Shalit, “On calibration and out-of-domain generalization,” *Advances in neural information processing systems*, vol. 34, pp. 2215–2227, 2021.
- [21] C. Henning, F. D’Angelo, and B. F. Grewe, “Are Bayesian neural networks intrinsically good at out-of-distribution detection?” *arXiv preprint arXiv:2107.12248*, 2021.
- [22] A. Kumar, S. Sarawagi, and U. Jain, “Trainable calibration measures for neural networks from kernel mean embeddings,” in *International Conference on Machine Learning*. PMLR, 2018, pp. 2805–2814.
- [23] C. Choi, F. Tajwar, Y. Lee, H. Yao, A. Kumar, and C. Finn, “Conservative prediction via data-driven confidence minimization,” *arXiv preprint arXiv:2306.04974*, 2023.
- [24] A. Fisch, T. Jaakkola, and R. Barzilay, “Calibrated selective classification,” *arXiv preprint*

arXiv:2208.12084, 2022.

- [25] C. Guo, G. Pleiss, Y. Sun, and K. Q. Weinberger, “On calibration of modern neural networks,” in *International conference on machine learning*. PMLR, 2017, pp. 1321–1330.
- [26] L. Tao, Y. Zhu, H. Guo, M. Dong, and C. Xu, “A benchmark study on calibration,” *arXiv preprint arXiv:2308.11838*, 2023.
- [27] D. Tran, J. Liu, M. W. Dusenberry, D. Phan, M. Collier, J. Ren, K. Han, Z. Wang, Z. Mariet, H. Hu *et al.*, “Plex: Towards reliability using pretrained large model extensions,” *arXiv preprint arXiv:2207.07411*, 2022.
- [28] H. S. Yoon, J. T. J. Tee, E. Yoon, S. Yoon, G. Kim, Y. Li, and C. D. Yoo, “ESD: Expected squared difference as a tuning-free trainable calibration measure,” *arXiv preprint arXiv:2303.02472*, 2023.
- [29] J. Mukhoti, V. Kulharia, A. Sanyal, S. Golodetz, P. Torr, and P. Dokania, “Calibrating deep neural networks using focal loss,” *Advances in Neural Information Processing Systems*, vol. 33, pp. 15 288–15 299, 2020.
- [30] A. Karandikar, N. Cain, D. Tran, B. Lakshminarayanan, J. Shlens, M. C. Mozer, and B. Roelofs, “Soft calibration objectives for neural networks,” *Advances in Neural Information Processing Systems*, vol. 34, pp. 29 768–29 779, 2021.
- [31] D. Hendrycks, M. Mazeika, and T. Dietterich, “Deep anomaly detection with outlier exposure,” *arXiv preprint arXiv:1812.04606*, 2018.
- [32] Y. Geifman, “Selectivenet: A deep neural network with an integrated reject option,” in *International conference on machine learning*. PMLR, 2019, pp. 2151–2159.
- [33] Y. Geifman and R. El-Yaniv, “Selective classification for deep neural networks,” *Advances in neural information processing systems*, vol. 30, 2017.
- [34] L. Huang, C. Zhang, and H. Zhang, “Self-adaptive training: Beyond empirical risk minimization,” *Advances in neural information processing systems*, vol. 33, pp. 19 365–19 376, 2020.
- [35] A. Pugnana, L. Perini, J. Davis, and S. Ruggieri, “Deep neural network benchmarks for selective classification,” *arXiv preprint arXiv:2401.12708*, 2024.
- [36] J. Huang, S. Park, and O. Simeone, “Calibration-aware Bayesian learning,” in *2023 IEEE 33rd International Workshop on Machine Learning for Signal Processing (MLSP)*. IEEE, 2023, pp. 1–6.

- [37] A. Krizhevsky, V. Nair, and G. Hinton, “Cifar-10 (Canadian institute for advanced research),” 2010.
- [38] S. Liang, Y. Li, and R. Srikant, “Principled detection of out-of-distribution examples in neural networks,” *CoRR*, *abs/1706.02690*, vol. 1, 2017.
- [39] O. Bohdal, Y. Yang, and T. Hospedales, “Meta-calibration: Learning of model calibration using differentiable expected calibration error,” *arXiv preprint arXiv:2106.09613*, 2021.
- [40] C. Wang, “Calibration in deep learning: A survey of the state-of-the-art,” *arXiv preprint arXiv:2308.01222*, 2023.
- [41] M. H. DeGroot and S. E. Fienberg, “The comparison and evaluation of forecasters,” *Journal of the Royal Statistical Society: Series D (The Statistician)*, vol. 32, no. 1-2, pp. 12–22, 1983.
- [42] M. P. Naeini, G. Cooper, and M. Hauskrecht, “Obtaining well calibrated probabilities using Bayesian binning,” in *Proceedings of the AAAI conference on artificial intelligence*, vol. 29, no. 1, 2015.
- [43] C. Blundell, J. Cornebise, K. Kavukcuoglu, and D. Wierstra, “Weight uncertainty in neural network,” in *International conference on machine learning*. PMLR, 2015, pp. 1613–1622.
- [44] Y. Gal and Z. Ghahramani, “Dropout as a Bayesian approximation: Representing model uncertainty in deep learning,” in *international conference on machine learning*. PMLR, 2016, pp. 1050–1059.
- [45] S. Mohamed, M. Rosca, M. Figurnov, and A. Mnih, “Monte carlo gradient estimation in machine learning,” *The Journal of Machine Learning Research*, vol. 21, no. 1, pp. 5183–5244, 2020.
- [46] C. Geng, S.-j. Huang, and S. Chen, “Recent advances in open set recognition: A survey,” *IEEE Transactions on Pattern Analysis and Machine Intelligence*, vol. 43, no. 10, pp. 3614–3631, 2020.
- [47] J. Ren, P. J. Liu, E. Fertig, J. Snoek, R. Poplin, M. Depristo, J. Dillon, and B. Lakshminarayanan, “Likelihood ratios for out-of-distribution detection,” *Advances in neural information processing systems*, vol. 32, 2019.
- [48] D. Hendrycks and K. Gimpel, “A baseline for detecting misclassified and out-of-distribution examples in neural networks,” *arXiv preprint arXiv:1610.02136*, 2016.
- [49] Y. Polyanskiy and Y. Wu, “Information theory: From coding to learning,” *Book draft*, 2022.
- [50] S. P. Boyd and L. Vandenberghe, *Convex optimization*. Cambridge university press, 2004.

- [51] D. W. Scott, *Multivariate density estimation: Theory, practice, and visualization*. John Wiley & Sons, 2015.
- [52] S. Zagoruyko and N. Komodakis, “Wide residual networks,” *arXiv preprint arXiv:1605.07146*, 2016.
- [53] A. Kumar, P. S. Liang, and T. Ma, “Verified uncertainty calibration,” *Advances in Neural Information Processing Systems*, vol. 32, 2019.
- [54] T. Raviv, S. Park, O. Simeone, and N. Shlezinger, “Modular model-based Bayesian learning for uncertainty-aware and reliable deep MIMO receivers,” in *2023 IEEE International Conference on Communications Workshops (ICC Workshops)*. IEEE, 2023, pp. 1032–1037.
- [55] M. Falkiewicz, N. Takeishi, I. Shekhzadeh, A. Wehenkel, A. Delaunoy, G. Louppe, and A. Kalousis, “Calibrating neural simulation-based inference with differentiable coverage probability,” *Advances in Neural Information Processing Systems*, vol. 36, 2024.
- [56] L. Li, E. Piccoli, A. Cossu, D. Bacciu, and V. Lomonaco, “Calibration of continual learning models,” *arXiv preprint arXiv:2404.07817*, 2024.
- [57] F. T. Liu, K. M. Ting, and Z.-H. Zhou, “Isolation forest,” in *2008 IEEE 8th International Conference on Data Mining*. IEEE, 2008, pp. 413–422.
- [58] B. Schölkopf, J. C. Platt, J. Shawe-Taylor, A. J. Smola, and R. C. Williamson, “Estimating the support of a high-dimensional distribution,” *Neural computation*, vol. 13, no. 7, pp. 1443–1471, 2001.
- [59] D. O. Loftsgaarden and C. P. Quesenberry, “A nonparametric estimate of a multivariate density function,” *The Annals of Mathematical Statistics*, vol. 36, no. 3, pp. 1049–1051, 1965.
- [60] A. Paszke, S. Gross, F. Massa, A. Lerer, J. Bradbury, G. Chanan, T. Killeen, Z. Lin, N. Gimelshein, L. Antiga *et al.*, “Pytorch: An imperative style, high-performance deep learning library,” *Advances in neural information processing systems*, vol. 32, 2019.
- [61] D. Hendrycks, M. Mazeika, and T. Dietterich, “Deep anomaly detection with outlier exposure,” *Proceedings of the International Conference on Learning Representations*, 2019.

Algorithm 1 SCBNN-OCM Training Procedure

Input: Training data set \mathcal{D}^{tr} , uncertainty data set \mathcal{D}^u , validation data set \mathcal{D}^{val} , ensemble size R^{tr} , prior distribution $p(\theta)$, step size α , hyperparameters $\beta, \lambda, \gamma, \eta$

Output: variational parameter vector $\varphi^{\text{CBNN-OCM}}$ for CBNN-OCM; selector parameter vector $\phi^{\text{SCBNN-OCM}}$

Initialize the variational parameter $\varphi = [\mu, \rho]$ composed of mean vector μ and variance vector $\exp(\rho)$ that defines the distribution over the parameter vector θ assuming Gaussian VI for Bayesian learning.

```

1: while not done do     $\triangleleft$  CBNN  $\triangleright$ 
2:   Sample mini-batch  $\tilde{\mathcal{D}}^{\text{tr}}$  from  $\mathcal{D}^{\text{tr}}$ 
3:   for  $r = 1, \dots, R^{\text{tr}}$  do
4:     Draw  $\epsilon_r \sim \mathcal{N}(0_N, I_N)$  and reparameterize  $\theta_r \leftarrow \mu + \exp(\rho) \circ \epsilon_r$ 
5:     Compute stochastic gradient  $g_r = (\nabla_{\varphi} \theta_r) \nabla_{\theta_r} [\mathcal{L}(\theta_r | \tilde{\mathcal{D}}^{\text{tr}}) + \lambda \cdot \mathcal{E}(\theta_r | \tilde{\mathcal{D}}^{\text{tr}})]$ 
6:   end for
7:   Update  $\varphi \leftarrow \varphi - \alpha \left( \frac{1}{R^{\text{tr}}} \sum_{r=1}^{R^{\text{tr}}} g_r + \beta \frac{|\tilde{\mathcal{D}}^{\text{tr}}|}{|\mathcal{D}^{\text{tr}}|} \cdot \nabla_{\varphi} \text{KL}(q(\theta | \varphi) \| p(\theta)) \right)$ 
8: end while
9: while not done do     $\triangleleft$  CBNN-OCM  $\triangleright$ 
10:  Sample mini-batch  $\tilde{\mathcal{D}}^{\text{tr}}$  from  $\mathcal{D}^{\text{tr}}$ ,  $\tilde{\mathcal{D}}^u$  from  $\mathcal{D}^u$ 
11:  for  $r = 1, \dots, R^{\text{tr}}$  do
12:    Draw  $\epsilon_r \sim \mathcal{N}(0_N, I_N)$  and reparameterize  $\theta_r \leftarrow \mu + \exp(\rho) \circ \epsilon_r$ 
13:    Compute stochastic gradient  $g_r = (\nabla_{\varphi} \theta_r) \nabla_{\theta_r} [\mathcal{L}(\theta_r | \tilde{\mathcal{D}}^{\text{tr}}) + \lambda \cdot \mathcal{E}(\theta_r | \tilde{\mathcal{D}}^{\text{tr}}) + \gamma \cdot \mathcal{C}(\theta_r | \tilde{\mathcal{D}}^u)]$ 
14:  end for
15:  Update  $\varphi \leftarrow \varphi - \alpha \left( \frac{1}{R^{\text{tr}}} \sum_{r=1}^{R^{\text{tr}}} g_r + \beta \frac{|\tilde{\mathcal{D}}^{\text{tr}}|}{|\mathcal{D}^{\text{tr}}|} \cdot \nabla_{\varphi} \text{KL}(q(\theta | \varphi) \| p(\theta)) \right)$ 
16: end while
17: while not done do     $\triangleleft$  SCBNN-OCM  $\triangleright$ 
18:  Sample mini-batch  $\tilde{\mathcal{D}}^{\text{val}}$  from  $\mathcal{D}^{\text{val}}$ 
19:  for  $r = 1, \dots, R^{\text{tr}}$  do
20:    Sample  $\theta_r \sim q(\theta | \varphi)$  to compute  $\bar{r}$  and  $\bar{s}$  as defined in (37) and (38)
21:  end for
22:  Compute stochastic gradient
    
$$g_{\phi} = \nabla_{\phi} \left[ \tilde{\mathcal{E}}^{\text{S-Cal}}(\phi | \mathcal{D}^{\text{val}}) - \eta \cdot \sum_{x \in \mathcal{D}^{\text{val}}} \log \tilde{g}(\bar{r}(x | \varphi), \bar{s}(x | \varphi) | \phi) \right]$$

23:  Update  $\phi \leftarrow \phi - \alpha \cdot g_{\phi}$ 
24: end while
25: return  $\varphi, \phi$ 

```

Algorithm 2 SCBNN-OCM Inference Procedure

Input: Test input x , ensembling size R^{te} , hyperparameter τ , variational parameter vector

$\varphi^{\text{CBNN-OCM}}$ for CBNN-OCM; selector parameter vector $\phi^{\text{SCBNN-OCM}}$

Output: hard decision $\hat{y}(x)$ with corresponding confidence $r(x)$ for the selected inputs

- 1: **for** $r = 1, \dots, R^{\text{te}}$ **do**
 - 2: Sample $\theta_r \sim q(\theta | \varphi^{\text{CBNN-OCM}})$ to compute \bar{r} and \bar{s} as defined in (37) and (38)
 - 3: **end for**
 - 4: Compute the relaxed selector output $\tilde{g}(\bar{r}, \bar{s} | \phi^{\text{SCBNN-OCM}})$
 - 5: **if** $\tilde{g}(\bar{r}, \bar{s} | \phi^{\text{SCBNN-OCM}}) \geq \tau$ **then**
 - 6: **return** select; yield label $y' \in \mathcal{Y}$ that is associated with \bar{r} (see (37))
 - 7: **else**
 - 8: **return** reject.
 - 9: **end if**
-